Journal of Physics and Chemistry of Solids 75 (2014) 583–587

Contents lists available at ScienceDirect

Journal of Physics and Chemistry of Solids

journal homepage: www.elsevier.com/locate/jpcs

Weak localization and electron–electron scattering in fluorine-doped SnO_2 random nanobelt thin films

Cleber A. Amorim [a,*], Cleocir J. Dalmaschio [b], André L.R. Melzi [a], Edson R. Leite [b], Adenilson J. Chiquito [a]

[a] Transporte Eletrônico em Nanoestruturas – NanoLab, Departamento de Física, Universidade Federal de São Carlos – UFSCar, Brazil
[b] Laboratório Interdisciplinar de Eletroquímica & Ceramica – LIEC, Departamento de Química, Universidade Federal de São Carlos – UFSCar, Brazil

ARTICLE INFO

Article history:
Received 26 August 2013
Received in revised form
25 December 2013
Accepted 6 January 2014
Available online 16 January 2014

Keywords:
A. Nanostructures
A. Oxides
D. Electrical properties
D. Magnetic properties
D. Transport properties

ABSTRACT

Electronic properties of self-assembled high crystalline quality fluorine-doped tin oxide (FTO) nanobelts were studied. We report the experimental transport data of a thin film made using a dispersion of these single-crystal nanobelts. We have shown that the theory of weak localization in a weak disorder regime provides a reasonable description of the observed electrons' transport characteristics of fluorine doped tin oxide nanobelts thin films. Also, our results suggest that the macroscopic extrinsic disorder, related to the random distribution of nanobelts, does not give a noticeable contribution to the whole transport mechanism.

1. Introduction

The wide band gap SnO_2 (3.8 eV) is an intrinsic n-type semiconductor usually found in a rutile structure [1]. The coexistence of electronic conduction and optical transparency is a characteristic feature of this class of materials but as it is well known, SnO_2 electrical conductivity is unstable due to the reaction of oxygen vacancies in the SnO_2 and the environment oxygen [2]. In addition, low carrier concentrations and consequently high resistivities of the undoped SnO_2 make it unsuitable for transparent and conducting coatings [3]. The electrical properties of thin films and bulk SnO_2 are dominated by different transport mechanisms: thermally activated process (including variable range hopping [4,5] and diffusive transport [4,6]. These mechanisms are associated with different conditions such as disorder, size of grains and potential barriers between them, doping, concentration of vacancies, for instance [7]. As above-mentioned, the primary source of carriers is associated with oxygen vacancies which cannot be controlled. However, the electrical conductivity control and enhancement can be achieved by doping SnO_2 with different impurities such as Zn, Sb, In and F [8,9]. In fact, Shanthi et al. showed that 57 at% FTO films present excellent resistivity ($< 10^{-3}\ \Omega$ cm) and high visible transparency ($> 88\%$) [10] when compared to ITO. More recently a comparative study between ITO and FTO films proposed by Aouaj et al. presented electrical resistivity of about 8×10^{-4} and $6 \times 10^{-4}\ \Omega$ cm for ITO (6% of Sn) and FTO (2.5% of F), respectively. Additionally, high optical transparency in the visible region and high near infrared reflectivity were observed in the literature [11]. Such properties make FTO interesting and a strong candidate to replace the usual TCO's.

On the other hand, SnO_2-based nanomaterials (nanorods, nanowires and nanobelts) have received extensive interest for use in gas/chemical sensors, transparent and flexible electronics, memories and integrated logic circuits [3,12–14]. These nanostructures are usually grown by the well known self-organized processes such as vapor–solid (VS) or vapor–liquid–solid (VLS) [15] showing high crystalline quality. Some of the conditions determining the conduction mechanisms pointed above are not present in these high quality nanostructures but disorder is always present and plays a fundamental role [16,17]. Electrons subjected to a random potential are not able to move freely through the system if either potential fluctuations due to disorder exceed a critical value or the electron energy is lower than the characteristic potential fluctuation [18,19]. Anderson's localization theory says that disorder plays a fundamental role in transport of charges leading to strong localization of carriers [20]. On the other hand, when a material shows a phase-breaking length larger than the localization length (in the limit of weak disorder $k_F l \gg 1$) the system is said to be in the weakly localized regime [21]. At this point is worth to remember that most devices with nanobelts are made by dispersing a large amount of them resulting in thin film structure. Then, considering the different degrees of disorder in samples due to growth processes, doping or device construction we can suppose that conduction mechanisms should be influenced.

* Corresponding author.

0022-3697/$ - see front matter © 2014 Elsevier Ltd. All rights reserved.
http://dx.doi.org/10.1016/j.jpcs.2014.01.003

In this paper we present transport and magnetotransport measurements of thin film fluorine doped tin oxide nanobelts. This system presents two different disorder sources, at least: an intrinsic disorder due to each nanobelt and an extrinsic disorder arising from random dispersion of nanobelts forming the thin film device. The results showed a localized character of the resistivity at low temperatures as evidenced by the presence of negative temperature resistance coefficient at temperatures lower than 15 K. Magneto-transport data showed directly the presence of weak-localization features enabling us to study parameters such as localization length and phase-breaking length. Additionally, electron–electron and electron–boundary scattering mechanisms were identified as the source of dephasing mechanisms. The extrinsic disorder seems to be not important to the transport in our samples as we will discuss in the following.

2. Experimental details

The samples were grown by carbothermal evaporation associated with the VS mechanism and NH_4F as a fluorine source. The tin source was the SnO_2 powder (Aldrich, >325 mesh, purity $>99.9\%$) which was mixed with graphite (Aldrich, $>20\,\mu m$, purity $>99\%$) 95:5 in weight, respectively by using a ball mill for 24 h. This mixture was placed in a melting pot and then it was inserted in a center of a horizontal tube furnace of alumina 100 cm (Lindberg-Blue M), where the temperature, gas flux and evaporation time were controlled in order to obtain the best conditions for the synthesis. Close to the tube ends was placed an alumina boat with 0.5 g NH_4F. The tube atmosphere was controlled during all the synthesis procedure. From room temperature to 600 °C an inert atmosphere was used, keeping 100 SCCM N_2 flow. From 600 °C to the end of the synthesis time a controlled O_2 quantity was admitted in both tube sides. The synthesis was carried out at 1200 °C for 2 h, using a 10 °C/min as heating rate. The white material collected was structurally and electrically characterized. The crystal structure was investigated by X-ray diffraction (XRD) using a Rigaku diffractometer model DMAX 2500PC, with Cu–Kα radiation ($\lambda=1.54056$ Å) at 40 kV and 150 mA. Microanalysis and microstructure characterization were performed by scanning electron microscope (SEM) FEI INSPECT F50 equipped with an energy dispersive X-ray spectrometer EDX.

A solution of nanobelts+ethanol has been prepared for FTO thin film nanobelts device construction. This solution was left to decant on thermally oxidized Si wafer an oxide layer SiO_2 of 500 nm thickness where interdigitated electrodes were microfabricated using lithographic techniques (Au/Ni–In, 70–30 nm). The final device was inserted in a tube furnace filled with an inert argon atmosphere at 450 °C for 10 min. The transport measurements were carried out at different temperatures from 10 to 300 K using a closed cycle helium cryostat and at a pressure lower than 5×10^{-7} mbar. Temperature dependent resistivity was measured using standard low frequency lock-in technique ($f=13$ Hz) with a Keithley 6221 as a current source. Magnetoresistance measurements were carried out by increasing and decreasing B using a Model EM7-HV Lakeshore electromagnet and no hysteresis was observed. The current–voltage curves at different temperatures were obtained by using a Keithley 237 source meter unit.

The crystal structure of the bulk material was investigated by X-ray diffraction (XRD), and Miller indices are indicated on each diffraction peak in Fig. 1a for FTO structure (PDF # 41-1445). The observed peaks are in full agreement with results obtained by Varshney et al. In that work the authors depicted a Rietveld refinement of the powder diffraction data for SnO_2 nanoparticles [22]. We also conducted the refinement and the analysis confirmed a tetragonal structure ($a=b=4.741$ A $c=3.1883$ Å) with the space group $P4_2/mnm$; Sn^{4+}, O^{2-} and F^- were found on 2(a) and 4(f) sites, respectively. Fig. 1b shows the EDX spectrum which indicates the expected composition of FTO, except the carbon, which is associated with the carbon tape used as a substrate in the analysis. The microstructures were also characterized by SEM and the obtained images were used in quantitative analysis: EDX spectra reveal that the synthesized nanobelts are composed of Sn, O and F. The presence of F was clearly observed and the atomic ratio of F:Sn was estimated to be ~4%. The as-grown material is composed of long nanobelts as can be observed in Fig. 1c in accordance with the VS process in which the vapor deposition will occur preferentially in faces with high energy resulting in the elongated structures [23,24].

As a further evidence of fluorine incorporation in the SnO_2 lattice, resistance measurements were performed at different temperatures ($30\,°C<T<900\,°C$) in a simple device built with the woolly as-grown material: as the temperature increases, the samples show no resistance variation until 750 °C when it increases significantly (more than three decades). Resistance was also measured in the cool down process and remained at the higher observed value. Considering that 750 °C is close enough to the synthesis temperature (600 °C) the resistance increase is an evidence that fluorine atoms were really incorporated in the SnO_2 lattice. Otherwise – for instance, fluorine atoms were physically adsorbed on the FTO nanobelt' surfaces – they would be evaporated at much lower temperatures.

3. Discussion

The samples were initially investigated by temperature dependent resistivity measurements in order to study the conduction

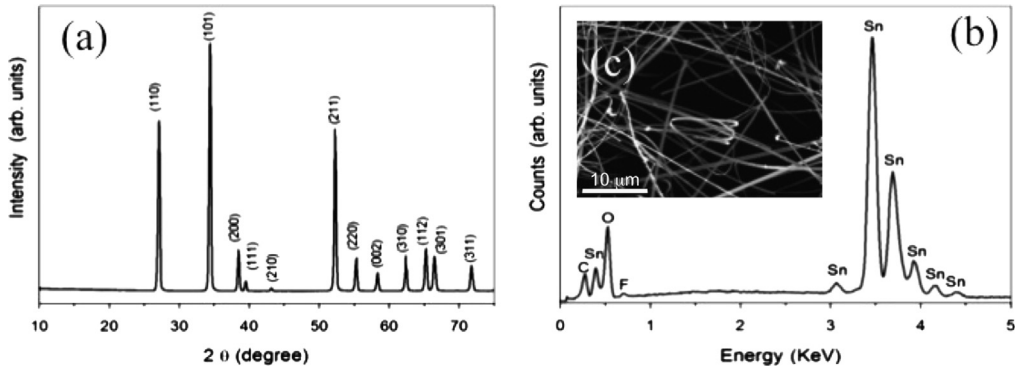

Fig. 1. Structural and chemical composition characterization of FTO samples. (a) XRD diffraction pattern (PDF # 41-1445) of FTO obtained by carbothermal reduction process, (b) EDX spectrum used to quantify the chemical composition of the samples and (c) SEM image of as-grown FTO samples showing nanobelts morphology with several micrometers of length.

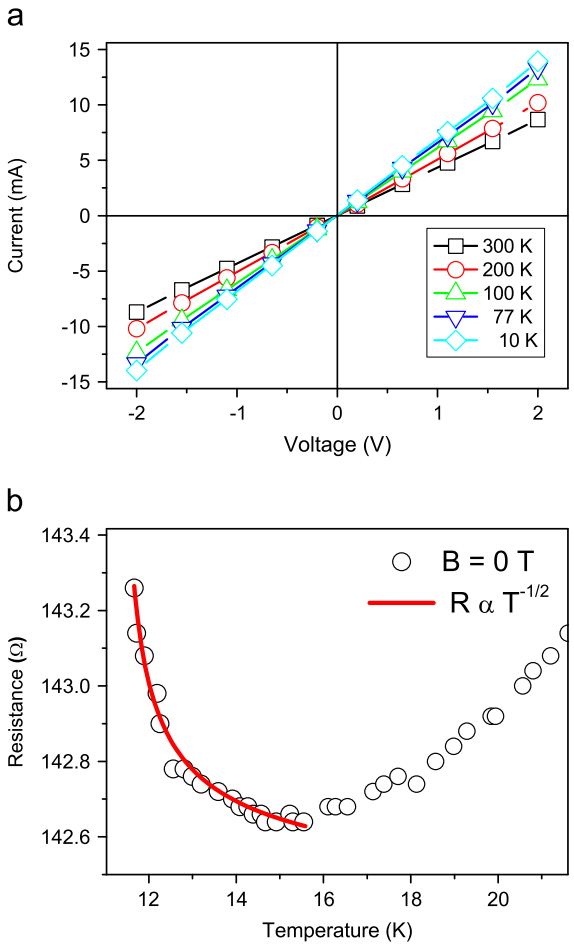

Fig. 2. In (a) current–voltage curves taken at different temperatures are displayed. In panel (b), temperature-dependent resistance measurements for the low temperature range at $B=0$ T. For $T<15$ K the experimental data are well described by the theoretical fit to the power law $R(T)=R_0+R_1/\sqrt{T}$.

regimes and the dominant scattering mechanisms present in the experimental devices. Fig. 2a shows the current–voltage characterization at different temperatures revealing ohmic characteristics. No potential contact (meaning energy barriers at the metal/FTO interfaces) was observed in all ranges of voltages/temperatures used. Fig. 2b depicts the resistivity data as a function of the temperature in low temperature range (10–15 K). In this range we found that the resistivity follows essentially a $T^{-1/2}$ law: $R(T)=142+0.52/\sqrt{T-11.3}$ which suggests that the electron–electron scattering mechanism is controlling the transport [25]. Simple activated and hopping laws were used to study the data but they lead us to unacceptable physical results. As it is well known, the $T^{-1/2}$ dependence of resistivity is expected for one-dimensional electron–electron scattering as discussed in the literature [26,27].

Usually, electron–electron scattering in disordered structures is accompanied by a weak localization effect at low temperatures and also related to the sample size. The disorder can be considered weak when $k_F\ell \gg 1$ where k_F is the Fermi wavelength and ℓ is the electron mean free path. For our sample, $k_F\ell=14.1$ estimated from free-electron theory [28]. Since the nanobelts width is reduced the boundary scattering becomes relatively more important than for larger belts because a significant portion of carriers are located near the belt boundaries. Thus, for small dimension nanobelts, the disorder coming from process like collisions with the boundaries provides the necessary disorder to randomize electron energy, resulting in a localized character for the transport as well as increasing the electron–electron interaction [27,29–31]. In the same way, the short temperature range in which we observed the electron–electron scattering mechanism can be explained based on the size of the nanostructures. Taking into account the cross-section of the nanobelts, the boundary scattering also becomes an important mechanism for the inelastic scattering at low temperatures [27,30,31]. For instance, Chiquito et al. showed that in 30 nm wide ITO nanobelts the electron–electron scattering was observed from 10 K to 77 K while in larger belts (1 μm wide) the Bloch–Grüneisen electron–phonon scattering mechanism was observed [29]. Similarly, Berengue et al. observed that 68 nm and 150 nm wide nanobelts exhibit electron–electron scattering from 10 K to 50 K and 10 K to 25 K, respectively [32]. From this discussion, in our FTO thin film of nanobelts the electron–electron and electron–boundary scattering effects provide the disorder for electrons transport and they should be considered as an intrinsic property. On the other hand, it seems that the disorder (extrinsic) arised from the random dispersion of nanobelts does not make a significative contribution for the whole conduction process.

In order to support the above discussion, we conducted several magneto-transport measurements. As well known in the presence of a weak disorder, the quantum coherence of time-reversal trajectories leads to the weak-localization regime [26]. Independent of the main mechanism of inelastic scattering of electrons, the phase-breaking time and length are power functions of temperature leading to a quantum correction for resistance which is quantified by the weak localization effect in a form $\Delta R \propto \ln(\tau_\phi k_B T/\hbar)$ where τ_ϕ is the phase-breaking time. From magnetic field dependent resistance curves Fig. 3a it was clear

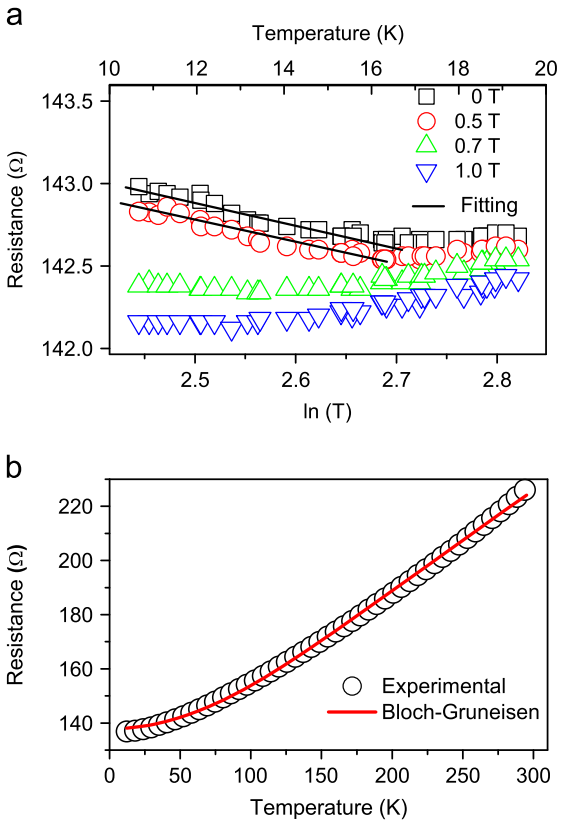

Fig. 3. (a) Linear dependence of resistance as a function of $\ln T$ and for different magnetic field intensities. The expected $\ln T$ dependence of resistivity is clearly observed until ~0.7 T and for higher magnetic fields, the resistance does not exhibit the negative temperature coefficient. (b) For $B=1.0$ T the sample exhibits a metallic–like behavior characterized by the acoustic phonon scattering (Bloch–Grüneisen theory).

that the quantum interference breaks when the magnetic field reaches $B \sim 0.7$ T. The phase-breaking length $L_\phi = \sqrt{D\tau_\phi}$ was estimated to be ~ 93 nm. The diffusion coefficient $D = v_F \ell/2 = 3.4 \times 10^{-3}$ m^2 s^{-1}, where v_F is the Fermi velocity. According to Datta et al. the critical magnetic field, B_C, needed to suppress the weak localization regime is given by [21]

$$B_C = \frac{h}{eWL_\phi}, \quad (1)$$

where W is the width of the nanobelts. Using the results presented in Fig. 3 we found $B_c = 0.53$ T in good agreement with the experimentally observed value. Below this value the weak localization regime should determine the behavior of the conductivity of the sample, as observed. From these results the negative temperature coefficient is a consequence of the weak localization regime where electron–electron and electron–boundary scattering mechanisms play a crucial role. In order to explore this result, Fig. 3b depicts the temperature-dependent resistance data for samples under $B = 1.0$ T (weak localization suppressed): we clearly observed a metallic behavior for the whole temperature range. These resistance data were then analyzed in the framework of the Bloch–Grüneisen theory based on the electron–acoustic phonon scattering mechanism. In fact, as temperature and electron excitation increase, the amount of scattering events experienced by the conduction electrons is increased as well, and as a consequence, the resistance increases. The resistance can be described by [33]

$$R(T) = R_0 + A\left(\frac{T}{\Theta_D}\right)^n \int_0^{T/\Theta_D} \frac{z^n e^z}{(e^z-1)^2}, \quad (2)$$

where A is an adjustable parameter proportional to the electron–phonon coupling, R_0 is the residual resistance and Θ_D is the Debye temperature. The fitting of the experimental data using Eq. (2) revealed $R_0 = 140\ \Omega$ and $\Theta_D = 542$ K in excellent agreement with the value found in the literature of $\Theta_D = 570$ K [34]. Furthermore, the analysis of the data revealed $n = 2$ while values commonly observed when acoustic phonon–electron scattering is present are in $3 < n < 5$ range. When the magnetic field above the critical value, B_C, was applied we effectively destroyed the weak localization regime but electron–electron and electron–boundary scattering processes remained unchanged. Then, the resistance data in Fig. 3b reflect more than one single scattering process. In fact, $n < 3,5$ in Eq. (2) indicates that there is another scattering mechanism in addition to the electron–acoustic phonon involved in the whole process (electron–electron and electron–boundary) [35]. Considering the parameters of the macroscopic device used in experiments, we obtain $B_c \sim 10^{-4}$ T in which it is far below the experimental results ($B = 0.7$ T). Considering the above discussion and the one-dimensional character of the transport, it seems that the electron transport on nanobelts thin film is dominated by the intrinsic processes occurring inside of nanobelts rather than in thin film as a macroscopic three-dimensional structure.

4. Conclusion

Electronic properties of self-assembled high crystalline quality fluorine-doped tin oxide nanobelts were studied. We report the experimental data and the related analysis on the resistance and magnetoresistance of a thin film made using a dispersion of these single-crystal nanobelts. The temperature dependence of the electrical resistance was studied from 10 to 300 K, and different conduction mechanisms were observed. We have shown that the theory of weak localization in a weak disorder regime provides a reasonable description of the observed electrons' transport characteristics of FTO thin films. Also, our results suggest that the macroscopic extrinsic disorder, related to the random distribution of nanobelts, does not give a noticeable contribution to the whole transport mechanism.

Acknowledgments

This work was financed by the Brazilian Agencies under Grants 141488/2010-7 and 302640/2010-0 (CNPq) and Grant 2011/10171-1 São Paulo Research Foundation (FAPESP). The author would like to thank Alan Rogério Ferreira Lima for Rietveld refinement.

References

[1] Z.L. Wang, Functional oxide nanobelts: materials, properties and potential applications in nanosystems and biotechnology, Annu. Rev. Phys. Chem. 55 (2004) 159.
[2] K.H. Kim, S.W. Lee, D.W. Shin, C.G. Park, Effect of antimony addition on electrical and optical properties of tin oxide film, J. Am. Ceram. Soc. 77 (4) (1994) 915.
[3] Q. Wan, E.N. Dattoli, W. Lu, Transparent metallic Sb-doped SnO_2 nanowires, Appl. Phys. Lett. 90 (22) (2007) 222107.
[4] T. Giraldi, M. Escote, P. Maciel, E. Longo, E. Leite, J. Varela, Transport and sensors properties of nanostructured antimony-doped tin oxide films, Thin Solid Films 515 (4) (2006) 2678.
[5] P. Gaiduk, A. Kozjevko, S. Prokopjev, C. Tsamis, A. Nylandsted Larsen, Structural and sensing properties of nanocrystalline SnO_2 films deposited by spray pyrolysis from a $SnCl_2$ precursor, Appl. Phys. A 91 (4) (2008) 667.
[6] M. Anwar, I.M. Ghauri, S.A. Siddiqi, AC conduction in amorphous thin films of SnO_2, J. Mater. Sci. 43 (18) (2008) 6049.
[7] T.A. Dauzhenka, V.K. Ksenevich, I.A. Bashmakov, J. Galibert, Origin of negative magnetoresistance in polycrystalline SnO_2 films, Phys. Rev. B 83 (16) (2011) 165309.
[8] K. Chopra, S. Major, D. Pandya, Transparent conductors: a status review, Thin Solid Films 102 (1) (1983) 1.
[9] T. Minami, S. Takata, H. Sonohara, Properties of transparent zinc–stannate conducting films prepared by radio frequency magnetron sputtering, J. Vac. Sci. Technol. A Vac. Surfaces Films 13 (3) (1995) 1095.
[10] S. Shanthi, C. Subramanian, P. Ramasamy, Preparation and properties of sprayed undoped and fluorine doped tin oxide films, Mater. Sci. Eng. B 57 (2) (1999) 127134.
[11] M.A. Aouaj, R. Diaz, a. Belayachi, F. Rueda, M. Abd-Lefdil, Comparative study of ITO and FTO thin films grown by spray pyrolysis, Mater. Res. Bull. 44 (7) (2009) 1458.
[12] J. Rebholz, C. Jaeschke, M. Hübner, U. Weimar, N. Barsan, D. Pham, L. Mädler, Chemistry, Conduction Mechanism in Undoped and Antimony Doped SnO_2 based FSP Gas Sensors (2012), p. 105.
[13] E.N. Dattoli, Q. Wan, W. Guo, Y. Chen, X. Pan, W. Lu, Fully transparent thin-film transistor devices based on SnO_2 nanowires, Nanoletters 7 (8) (2007) 2463.
[14] J.G. Lu, P. Chang, Z. Fan, Quasi-one-dimensional metal oxide materials, properties and applications, Mater. Sci. Eng. R Reports 52 (1–3) (2006) 4991.
[15] R.S. Wagner, W.C. Ellis, Vapor–liquid–solid mechanism of single crystal growth, Appl. Phys. Lett. 4 (5) (1964) 89.
[16] M. Kojima, H. Kato, A. Imai, A. Yoshida, Electronic conduction of tin oxide thin films prepared by chemical vapor deposition, J. Appl. Phys. 64 (4) (1988) 1902.
[17] D.H. Zhang, H.L. Ma, Scattering mechanisms of charge carriers in transparent conducting oxide films, Appl. Phys. A Mater. Sci. Process. 62 (5) (1996) 487.
[18] Y.A. Pusep, A.J. Chiquito, S. Mergulhao, A.I. Toropov, Parallel conductivity of random GaAs/AlGaAs superlattices in regime of controlled vertical disorder, J. Appl. Phys. 92 (2002) 3830.
[19] A. Chiquito, Y. Pusep, G. Gusev, A. Toropov, Quantum interference in intentionally disordered doped GaAs/Al_xGa_{1-x}As superlattices, Phys. Rev. B 66 (3) (2002) 035323.
[20] E. Abrahams, P.W. Anderson, D.C. Licciardello, T.V. Ramakrishnan, Scaling theory of localization: absence of quantum diffusion in two dimensions, Phys. Rev. Lett. 42 (10) (1979) 673.
[21] S. Datta, Electronic Transport in Mesoscopic Systems, Cambridge University Press, Cambridge, 1997.
[22] D. Varshney, K. Verma, Effect of stirring time on size and dielectric properties of SnO_2 nanoparticles prepared by co-precipitation method, J. Mol. Struct. 1034 (2013) 216.
[23] O.M. Berengue, R.A. Simon, A.J. Chiquito, C.J. Dalmaschio, E.R. Leite, H.A. Guerreiro, F.E.G. Guimaraes, Semiconducting Sn_3O_4 nanobelts: growth and electronic structure, J. Appl. Phys. 107 (3) (2010) 033717.
[24] A.J.C. Lanfredi, R.R. Geraldes, O.M. Berengue, E.R. Leite, A.J. Chiquito, Electron transport properties of undoped SnO_2 monocrystals, J. Appl. Phys. 105 (2) (2009) 023708.
[25] J. Heremans, C. Thrush, D. Morelli, M.-C. Wu, Resistance, magnetoresistance, and thermopower of zinc nanowire Composites, Phys. Rev. Lett. 91 (7) (2003) 076804.
[26] B.L. Altshuler, A.G. Aranov, Electron–Electron Interaction in Disordered Systems, Elsevier, New York, 1985.

[27] D. Beutler, N. Giordano, Localization and electron–electron interaction effects in thin Bi wires and films, Phys. Rev. B 38 (1) (1988) 8.
[28] A.J. Chiquito, A.J.C. Lanfredi, E.R. Leite, One-dimensional character of Sn doped In_2O_3 nanowires probed by magnetotransport measurements, J. Phys. D Appl. Phys. 41 (4) (2008) 045106.
[29] A.J. Chiquito, A.J.C. Lanfredi, R.F.M.D. Oliveira, L.P. Pozzi, E.R. Leite, Electron dephasing and weak localization in Sn doped In_2O_3 nanowires, Nanoletters 7 (5) (2007) 1439.
[30] J.J. Lin, J.P. Bird, Recent experimental studies of electron dephasing in metal and semiconductor mesoscopic structures, J. Phys. Condens. Matter 14 (18) (2002) R501.
[31] D. Natelson, R. Willett, K. West, L. Pfeiffer, Molecular-scale metal wires, Solid State Commun. 115 (5) (2000) 269.
[32] O.M. Berengue, A.J.C. Lanfredi, L.P. Pozzi, J.F.Q. Rey, E.R. Leite, A.J. Chiquito, Magneto resistance in Sn-doped In_2O_3 nanowires, Nanoscale Res. Lett. 4 (8) (2009) 921.
[33] J.M. Ziman, Electrons and Phonons, Claredon Press, Oxford, 1960.
[34] P. Turkes, C. Pluntke, R. Helbig, Thermal conductivity of SnO_2 single crystals, J. Phys. C Solid State Phys. 13 (26) (1980) 4941.
[35] L. Qiao, X. Bi, Nanostructure and performance of $PtLaNiO_3$ composite film for ferroelectric film devices, Acta Mater. 57 (14) (2009).